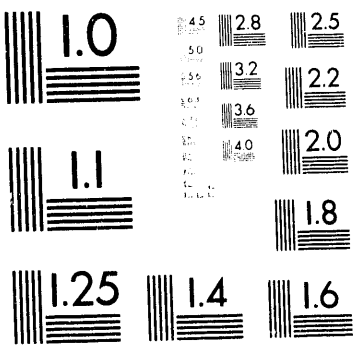
1.0
1.1
1.25
1.4
1.6
1.8
2.0
2.2
2.5
2.8
3.2
3.6
4.0
4.5
5.0
5.6

1 of 1

CONF-8808147--25

Jet Production in $\gamma\gamma$ Interactions at PEP

AC02-85ER40194

H. Aihara, M. Alston-Garnjost, R.E. Avery, A. Barbaro-Galtieri, A.R. Barker, B.A. Barnett, D.A. Bauer, A. Bay, G.J. Bobbink, C.D. Buchanan, A. Buijs, D.O. Caldwell, H-Y. Chao, S-B. Chun, A.R. Clark, G.D. Cowan, D.A. Crane, O.I. Dahl, M. Daoudi, K.A. Derby, J.J. Eastman, P.H. Eberhard, T.K. Edberg, A.M. Eisner, F.C. Erné, K.H. Fairfield, J.M. Hauptman, W. Hofmann, J. Hylen, T. Kamae, H.S. Kaye, R.W. Kenney, S. Khacheryan, R.R. Kofler, W.G.J. Langeveld, J.G. Layter, W.T. Lin, F.L. Linde, S.C. Loken, G.R. Lynch, R.J. Madaras, B.D. Magnuson, G.E. Masek, L.G. Mathis, J.A.J. Matthews, S.J. Maxfield, E.S. Miller, W. Moses, D.R. Nygren, P.J. Oddone, H.P. Paar, S.K. Park, D.E. Pellett, M. Pripstein, M.T. Ronan, R.R. Ross, F.R. Rouse, K.A. Schwitkis, J.C. Sens, G. Shapiro, B.C. Shen, J.R. Smith, J.S. Steinman, R.W. Stephens, M.L. Stevenson, D.H. Stork, M.G. Strauss, M.K. Sullivan, T. Takahashi, S. Toutounchi, R. van Tyen, W. Vernon, W. Wagner, E.M. Wang, Y-X. Wang, W.A. Wenzel, Z.R. Wolf, H. Yamamoto, S.J. Yellin and C. Zeitlin

TPC/Two-Gamma Collaboration

Lawrence Berkeley Laboratory, Berkeley, California 94720
University of California, Davis,California 95616
University of California Intercampus Institute for Research at Particle Accelerators, Stanford, California 94305
University of California, Los Angeles, California 90024
University of California, Riverside, California 92521
University of California, San Diego, California 92093
University of California, Santa Barbara, California 93106
Ames Laboratory, Iowa State University, Ames, Iowa 50011
Johns Hopkins University, Baltimore, Maryland 21218
University of Massachusetts, Amherst, Massachusetts 01003
National Institute for Nuclear and High Energy Physics, Amsterdam, The Netherlands
University of Tokyo, Tokyo, Japan

Submitted to the XXIV International Conference on High Energy Physics
Munich, August 4-10, 1988

ABSTRACT

We have used the TPC/Two-Gamma Facility at the SLAC e^+e^- storage ring PEP to study the photon-photon reaction $e^+e^- \rightarrow e^+e^- + hadrons$, in both the single-tagged mode (one outgoing $e^\pm$ detected) and the untagged mode (neither $e^\pm$ detected). A thrust algorithm was used to find the jet axis in the hadronic center-of-mass, and this axis was used to calculate the transverse momentum with respect to the $\gamma\gamma$ collision axis (p_t). The (preliminary) p_t and thrust distributions of both tagged and untagged data are well-described by the predictions of vector meson dominance (VDM) at low p_t. For $3 < p_t < 4.5\,\mathrm{GeV}$, the tagged data are consistent with the prediction of the Quark Parton Model (QPM). In the intermediate region - $1.5 < p_t < 3\,\mathrm{GeV}$ - an excess of events is seen in both samples. The p_t and event topology of these excess events are compared to a 3-jet model based on QCD.

1 Introduction

Many aspects of inclusive hadron production in photon-photon collisions have been studied at e^+e^- colliders in recent years [1,2]. Measurement of the total cross section, photon structure function, and transverse momentum distributions have all suggested the existence of two major contributions to the reaction $e^+e^- \rightarrow e^+e^-$+hadrons. These two contributions are dominant in different kinematic regions: the "soft" regime where one (or both) of the γ's fluctuates into a vector meson which subsequently interacts, and the "hard" regime where photons couple directly to quarks which then fragment to produce the final state hadrons. Models have been developed which correspond to the "soft" and "hard" regimes. Although there is substantial overlap between these kinematic regimes, the incoherent sum of the two models has successfully reproduced many of the features of data.

Previous results on the total cross section [3,4] and structure function have concentrated on events where one of the photons is quasi-real and constitutes a target for the highly virtual (spacelike) probe photon. The invariant mass squared of the probe photon ($-Q^2$) is a measure of momentum transfer from the target photon and is used to distinguish between the two regimes. The $\gamma\gamma$ cross section at low Q^2 follows a Vector Dominance Model (VDM) form factor which is a generalization of the ρ-pole form factor to include higher mass vector mesons. This model is consistent with our "soft" regime picture of vector meson scattering and shows itself in the sharp fall of the form factor with Q^2. But the data also show a contribution which is characteristic of hard scattering; it is present at all Q^2 and dominant at high Q^2. The principal hard scattering or point-like interaction model is the Quark Parton Model (QPM). The cross section for the reaction $\gamma\gamma \rightarrow q\bar{q}$ is related to the QED process $\gamma\gamma \rightarrow \mu^+\mu^-$ by the factor $3\sum e_i^4$, where the sum runs over quark flavors, and where quark masses are used in place of the lepton masses. As expected, the QPM cross section falls off less sharply with increasing Q^2 than the VDM cross section. In addition, the structure function measurements clearly show the presence of a point-like component.

The total cross section and structure function are functions of Q^2, W (the invariant mass of $\gamma\gamma$ system) and $x = Q^2/(Q^2 + W^2)$. Another kinematic variable one can examine is the transverse momentum (p_t) distribu-

tion of hadrons with respect to the $\gamma\gamma$ axis. The observed single-particle p_t distribution at low p_t [5,6] is reminiscent of hadron-hadron scattering at low p_t as expected from VDM; however the data also show a high p_t tail, once again indicating the presence of a hard scattering mechanism. One generally interprets the source of high p_t particles to be the fragmentation of high p_t partons emerging from hard scattering. The transverse momentum of the final state partons is limited only by phase space in the hard scattering picture, whereas it is expected to be limited to typical hadronic values (300–400 MeV) in the soft regime, where the partons are bound in vector mesons. In e^+e^- annihilation events, partons manifest themseleves as jets of particles. The PLUTO collaboration [7] has examined jet production in $\gamma\gamma$ interactions, and a VDM+QPM model was found to be adequate to explain the jet p_t distributions in both the high and low p_t regions; however in the intermediate jet p_t region (1.5 to 3.0 GeV), the naive VDM+QPM model was insufficient to explain the data. The excess events in the data were also reported to have a more isotropic topology than predicted by the models. QCD predicts the existence of hard scattering diagrams beyond the first order QPM diagram [8,9,10]. These multijet diagrams produce two high p_t jets, similar to QPM, along with extra "beam pipe" jets going along the $\gamma\gamma$ axis (which is generally close to the beam axis). The resulting distribution of hadrons is more isotropic than in two-jet events, but it is not clear that such diagrams can fully account for the observed excess[9,10].

In e^+e^- storage rings, the two-photon reaction proceeds via emission of space-like photons by the incoming e^+ and e^-. Each photon and its mass can be tagged by detecting the corresponding $e^\pm$, and measurements can be classified according to the number (0, 1 or 2) of such "tags". One can also restrict one or both photons to being nearly on-shell, or quasi-real, by anti-tag cuts. In this paper we present preliminary results from a study of jet formation in $\gamma\gamma$ interactions for both the single tagged and untagged reactions. The data were taken with the TPC/2γ facility at the SLAC e^+e^- storage ring PEP, operated at a beam energy of 14.5 GeV. In our single-tag sample, one photon was anti-tagged, while in the untagged sample, both photons were anti-tagged.

The study of jets in $\gamma\gamma$ interactions is more complicated than the corresponding study in e^+e^- annihilation. First, since most of the available energy is carried away by the scattered electron and positron, the center-

of-mass energy of the $\gamma\gamma$ system is small compared to the full energy of the e^+e^- system. As a result the $\gamma\gamma$ system may not have enough energy to allow one to distinguish jets. Also, for $W <\sim 2$ GeV, $\gamma\gamma$ interactions frequently produce resonances. For these reasons one has to impose a minimum visible energy cut which will remove the majority of photon-photon events. Second, the two reacting photons generally do not have the same energy so that the $\gamma\gamma$ center of mass is moving in the lab frame. Since most jet finding algorithms rely on the back-to-back topology of the jets in the center of mass of the system, one needs to Lorentz transform the event to the center of mass of the visible hadrons, as the closest approximation to the $\gamma\gamma$ center of mass frame. Finally, in the case of untagged reactions, there are severe backgrounds from e^+e^- annihilation which must be subtracted statistically using Monte Carlo estimates. Despite these difficulties, one can reconstruct jets, and Monte Carlo studies indicate[11] that measured jet p_t is well correlated with the initial parton, p_t^{quark} (especially for jet $p_t > 1$ GeV). This measured jet p_t is generally less than the true p_t^{quark} due to particles which escape detection.

2 Detector and Event Selection

For this measurement, charged particles at angles greater than 350 mrad with respect to the beam axis were detected in the Time Projection Chamber (TPC), which simultaneously measured momentum and ionization energy loss, dE/dx. The 13.25 kilogauss magnetic field allowed a momentum resolution (at large polar angles), $\delta p/p = \sqrt{(.015)^2 + (0.006p)^2}$, where p is in Gev/c. Charged particles in the polar angle range of 28–180 mrad were detected in 15 planes of drift chambers arranged in 5 layers. Conventional cylindrical drift chambers at smaller and larger radii than the TPC were used to assist in triggering. Muon detectors covered 98% of 4π. Neutral particles at polar angles more than 700 mrad were detected in a hexagonal Geiger-mode calorimeter (HEX). Other calorimeters used at smaller angles were: proportional-mode Pole-Tip Calorimeters (PTC) covering the region from 300 to 600 mrad, lead/scintillator Shower Counters (SHW) between 100 and 180 mrad, and NaI crystals between 28 and 90 mrad. The latter two calorimeters were also used as tagging devices. Further details of the

TPC/2γ facility can be found in the literature[12,13]. The trigger for the single tag data required energy deposit in the NaI or SHW calorimeters in coincidence with a TPC track; the untagged data required a trigger with at least 2 charged particle tracks in the TPC. The integrated luminosity was $\simeq 62\ pb^{-1}$.

For the single-tag sample, we defined a tag to be a calorimeter deposition of at least 8 GeV in the NaI or SHW fiducial volume which matched to a reconstructed track in the forward drift chambers. The untagged sample in general has tighter cuts because it is more vulnerable to background than the tagged sample. In both samples a minimum of four charged tracks was required. In the tagged sample, we required two or more of the charged tracks to be in the TPC, while in the untagged sample we required at least four tracks to be in the TPC. At least one of the TPC tracks had to be identified as a hadron (or muon) by the TPC dE/dx and momentum measurements in the tagged sample, while for the untagged case, the minimum number of identified hadrons was three. The invariant mass of the observed final state, W_{vis} was required to be greater than 3.5 GeV for the single-tagged data and 4.0 GeV for the untagged data. Upper limits on W_{vis} to reduce background were set at 12 GeV in the tagged data and at 10 GeV in the untagged data. A p_t balance cut of 1 GeV (including the tag) was made in the tagged sample and 2 GeV in the untagged. For the tagged case, the absolute value of the net charge of the observed hadrons was required to be ≤ 2, and the total visible energy (including the tag) less than 23.2 GeV. Distorted Bhabha events in the untagged sample were rejected by requiring that the average energy of the charged tracks was less than 2 GeV. Antitagging was applied to both samples as follows: for the tagged case, there can be no energy cluster, E_{cal}, more than 4 GeV opposite to the tag in forward calorimeters and no E_{cal} more than 3 GeV in the central calorimeters. For the untagged case no E_{cal} more than 3 GeV is allowed in any of the calorimeters. This cut also helps to reduce the annihilation background.

Beam-gas backgrounds totalling roughly 3.5% in the tagged data and 9% in the untagged were subtracted using the sidebands of the vertex z distributions. Two other classes of backgrounds were estimated by Monte Carlo calculations and, when non-negligible, subtracted bin-by-bin from the data. These classes are: *(i)* e^+e^- annihilation into hadrons and τ pairs; *(ii)*

$\gamma\gamma$ production of τ pairs. Annihilation background in the tagged sample is negligible but there is 10% multihadronic and 0.1% τ pair contamination in the untagged sample. The $\gamma\gamma$ production of τ pairs was a 0.4% background in the tagged sample and 0.1% in the untagged data.

3 Results

The study of jet structure enables the dynamics of the otherwise unobservable quarks to be investigated. For this study the jet search is carried out in the hadronic rest frame (our best estimate of the $\gamma\gamma$ CMS frame). One of the jet finding procedures used is the thrust algorithm. Thrust is defined as

$$T = max\{\frac{\sum_i |p_{Li}|}{\sum_i |\vec{p_i}|}\}$$

where the value is maximized with respect to the choice of the quark axes. Thus the thrust algorithm maximizes the sum of the longitudinal momenta of the particles along the jet axis (assuming there are 2 back-to-back quarks in the event). The value of thrust ranges from 0.5 for perfectly isotropic events to 1 for extremely collimated two-jet events. The thrust axis provides a jet direction for the event. One can then divide the event into two hemispheres, and define jet momentum as

$$\vec{p}^{jet} = \sum_i \vec{p_i}$$

where the sum runs over all particles in the same hemisphere. Jet p_t is the transverse momentum of the jet with respect to the $\gamma\gamma$ axis. The $\gamma\gamma$ axis is assumed to be the beam axis in the untagged case. In the tagged case, the $\gamma\gamma$ axis is defined to be the direction of the momentum vector of the tagged photon in the hadronic rest frame. Jet p_t is defined as

$$p_t = |\vec{p}^{jet}| sin\theta^*$$

where θ^* is the polar angle between the thrust axis and the $\gamma\gamma$ direction in the hadronic rest frame.

The p_t^{quark} dependence of the $q\overline{q}$ in the QPM simulation is calculated using QED[8], and falls approximately as $p_t^{quark^{-4}}$. We have modeled the

VDM final state using Monte Carlo methods by generating $q\overline{q}$ pairs with limited p_t^{quark} according to the distribution

$$\frac{d\sigma}{dp_t^{quark^2}} \sim e^{-bp_t^{quark^2}}$$

In both cases, the $q\overline{q}$ are fragmented according to the Lund model[14]. Events were then passed through a full detector and trigger simulation (including the effects of secondary interactions), followed by the application of the same analysis used for the data. The normalization of VDM was chosen to match the data in the lowest p_t bin, and the parameter b was varied over the range of $2-8$.

Our preliminary results are presented in Figure 1 which shows the distribution of measured p_t in the data sample (corrected for the estimated background), along with the predicted distributions from the Monte Carlo simulations of both the VDM and QPM production mechanisms. Because it best reproduced the p_t distribution of the data at low p_t we have used the value b = 2 in the subsequent analysis. Also shown in Figure 1 are the curves for b = 5. The normalization of the Monte Carlo VDM (with b=2) to the untagged data required a VDM cross section of 240 nb; while the corresponding normalization in the tagged data was 300 nb, using a VDM form factor which was found to describe our cross section data well[4]. The untagged data are inconsistent with the simple (VDM + QPM) predictions for p_t in the range from ~1 to ~3 GeV where the model underestimates the data. For the tagged data the model is closer to the observed results; however an excess is also evident in the intermediate p_t range. This is consistent with results reported by other experiments[7].

In order to display the deviation of the data from the (VDM + QPM) prediction more graphically, we define

$$R'_{\gamma\gamma} = \frac{N(data) - N(background)}{N(QPM) + N(VDM)}.$$

The background term in the $R'_{\gamma\gamma}$ definition is negligible for the tagged sample, but in the untagged data the annihilation background is especially large at high p_t, approaching 50% above $p_t = 4$ GeV. $R'_{\gamma\gamma}$ is similar to the quantity $R_{\gamma\gamma}$ defined by the PLUTO collaboration but has the advantage of

showing the excess more directly and is less sensitive to detector acceptance effects at low p_t. Figure 2 shows $R'_{\gamma\gamma}$ for the untagged data and for the tagged data in two bins of Q^2. The value $R'_{\gamma\gamma} = 1$ obviously corresponds to perfect agreement with the VDM + QPM prediction. A significant excess in the range $2 < p_t < 3$ GeV is obvious in all of the plots, and appears to decrease with increasing Q^2. At the highest p_t, where there is no VDM contribution, $R'_{\gamma\gamma}$ is consistent with 1 in the tagged data, indicating that the QPM description is adequate at sufficiently high p_t. In the untagged sample the discrepancy decreases above 3 GeV, however the data above $p_t = 3.5$ are dominated by annihilation background and potential systematic errors, and a significant measurement is not currently available above $p_t = 3.5$ GeV.

We have searched for possible sources of systematic error in our analysis. The dominant source, particularly in the p_t region between 2 and 3 GeV, is the accuracy with which the Monte Carlo calculation simulates the shift between the true p_t^{quark} and the reconstructed p_t. Using the region below $p_t = 0.75$ GeV, where the data are reasonably close to the predictions of the model, we have compared numerous features of the data with the Monte Carlo model predictions. We find small, but significant, differences in the distributions of track momenta and angles. If we attribute these discrepancies to inadequacies in the combination of the fragmentation model and the detector and cut simulations, then there is a potential error in the Monte Carlo p_t scale. While further study is necessary to determine the extent to which this effect is actually present, we use it to estimate a preliminary systematic error which is p_t-dependent and reaches its largest value, $\sim 30\%$, between 2 and 3 GeV. Other sources of systematic uncertainty (integrated luminosity in the data, background subtraction, etc) total less than 15%.

In order to study the nature of the excess in more detail, we select a subset of the data with $2 < p_t < 3$ GeV. The VDM contribution to this sample is predicted by Monte Carlo estimates to be negligible, hence the QPM contribution is expected to dominate this data. Table 1 lists the number of events in the data samples in this range of p_t along with the number of events predicted by the QPM Monte Carlo. The fivefold excess of the data in the untagged sample and the twofold excess of the data in the tagged sample are unambiguously significant. No variation of model or fragmentation parameters can explain the excess data in the $2 < p_t < 3$ GeV region.

Figure 3 shows the thrust distributions of these (background subtracted) data along with histograms representing the corresponding thrust distributions predicted by the QPM Monte Carlo. It should be noted that we have arbitrarily scaled the QPM results to match the total events in the data; in the case of the untagged data sample the QPM results required a large scaling factor ($\simeq$5) due to the large excess of the data over the model. On the average,the data have lower thrust than the two-jet events produced in the QPM in this region. As mentioned earlier, multi-jet events will have a more spherical topology and lower thrust than two-jet events.

4 Comparison to a Three-Jet Model

Higher order QCD diagrams (Figure 4) were the first candidates to explain the observed excess at high p_t.In multi-jet events one (or both) of the incoming photons fluctuates into a $q\overline{q}$ pair and the quark (or the anti-quark) undergoes the hard scattering. For example in the three jet diagram of Figure 4a one of the photons becomes a $q\overline{q}$ followed by the reaction $\gamma q \rightarrow gq$. Using the hard scattering formalism, the three jet cross section can be written as

$$\frac{d\sigma_{\gamma\gamma}^{3jet}}{dp_t dQ^2} = \int_{x_{min}}^{1} dx f_{q/\gamma}(x) \frac{d\sigma_{\gamma q \rightarrow gq}}{dp_t dQ^2}$$

where $f_{q/\gamma}$ is the probability that the interacting quark carries the fraction x of split photon energy, and $d\sigma_{\gamma q \rightarrow gq}/dp_t dQ^2$ is the calculated hard scattering cross section from Feynman diagrams. The function $f_{q/\gamma}$ is related to the photon structure function by the relation

$$F_\gamma^2 = 2x \sum_i e_q^2 f_{q_i/\gamma}$$

where the sum runs over quark flavors. The measured structure function has a point-like and a hadronic contribution. The point-like piece can be calculated from QED and has an x-dependence which can be approximated by

$$f_{q/\gamma}^{QED} \sim x^2 + (1-x)^2$$

The hadronic piece cannot be calculated in perturbative QCD, but can be related to the measured pion structure function (with many assumptions)

and has the form

$$f_{q/\gamma}^{hadronic} \sim \frac{1-x}{x}$$

This contribution to the multi-jet cross section has been shown[9] to be comparable to the QPM contribution at p_t as high as 2 GeV in the single-hadron spectrum. Therefore it may be important to consider this contribution to the multi-jet cross section.

We have used the hard scattering formalism above and the subprocess cross section, $d\sigma_{\gamma q \to gq}/dp_t dQ^2$, given in Ref. 10 in a Monte Carlo event generator for the three-jet final state. A cut made at the generator level required the p_t of the quark and gluon involved in the hard scattering to be at least 2 GeV, guaranteeing that we remain in a region where the use of perturbation theory is valid. Both $f_{q/\gamma}^{hadronic}$ and $f_{q/\gamma}^{QED}$ were studied and, for the purpose of event generation, we used

$$f_{q/\gamma} = f_{q/\gamma}^{hadronic} + f_{q/\gamma}^{QED}$$

Events produced by the generator were subjected to the usual detector simulation and cuts. The cross section for the 3-jet process (determined by the generator program) was found to be much too small to explain the excess of events in the region $1.5 < p_t < 3$ GeV. This will be discussed in more detail below.

Quantifying the discrepancy between data and the two-jet model (VDM + QPM) is difficult in the range $1.5 < p_t < 2$ GeV because the contribution from VDM in this bin is sensitive to the generated p_t distribution (specifically to the slope parameter b in the exponential). In the following, therefore, we restrict ourselves to the region $2 < p_t < 3$ GeV where the contribution from VDM is negligible, independent of b, and is therefore ignored. Table 1 shows the numbers of events seen in the data samples (background subtracted in the untagged case) and expected from the QPM and 3-jet Monte Carlos (the Monte Carlo luminosities are adjusted to those of the data samples). It is clear that the combination of the QPM and 3-jet model cannot explain the number of events seen in the data.

Setting aside the question of the 3-jet normalization for the moment, we adopt the following approach for making event topology comparisons: we accept the absolute prediction from QPM for the number of 2-jet events, and adjust the normalization of the 3-jet events so that the total number

of data events in each sample is accounted for. Figure 5 shows the thrust distributions again, but now with histograms representing this new model. The agreement between data and the model is much better than in the previous comparison. The high-thrust end of the spectrum is dominated by 2-jet events and agrees well with the model. Further topology comparisons, including the use of a cluster-finding algorithm and a search for particles at small angles (perhaps indicative of beam-pipe jets), have been undertaken for the single-tagged data[11]. These comparisons yield results consistent with the results of the thrust analysis: the data are more compatible with the 2-jet + 3-jet model than with a 2-jet model alone.

5 Conclusion

In summary, we have compared the distribution of jet p_t in our data with Monte Carlo predictions based on a model which includes both VDM and QPM simulations. We observe the presence of significant excess data in the range $2 < p_t < 3$ GeV in comparison with this model. In this intermediate range of p_t the data exceeds the prediction by a factor of $\sim$5 in the untagged sample and by a factor of $\sim$2 in the tagged sample. There is evidence in the tagged data sample that this discrepency decreases with increasing Q^2. A 3-jet model based on QCD cannot account for the observed number of events, even when the hadronic component of the photon is included in the quark distribution function. However, the thrust distribution of the excess events agrees well with the predictions of this model in the range $2 < p_t < 3$ GeV even though the predicted size of the 3-jet contribution is roughly an order of magnitude too small to explain the observed excess. At the highest values of p_t the data are consistent with the predictions of the QPM, at least in the tagged data, although a contribution from multi-jet events is not ruled out. The low-p_t data are well-described by Monte Carlo events with a limited-p_t topology, in accordance with expectations for soft (vector meson) scattering.

We would like to thank the PEP staff and engineers for the productive running of the machine. This work was supported in part by the United States Department of Energy, the National Science Foundation, the Joint Japan-United States Collaboration in High Energy Physics, and the Foun-

dation for Fundamental Research in The Netherlands.

References

[1] C. Berger and W. Wagner, Phys. Rep. **146**, 1 (1987).

[2] H. Kolanoski, in *Two Photon Physics at e^+e^- Storage Rings* (Springer-Verlag, 1984).

[3] C. Berger *et al.*, Phys. Lett. **149B**, 421 (1984).

[4] H. Aihara *et al.*, in *VIII International Workshop on Photon-Photon Collisions* (1988, contributed paper).

[5] R. Brandelik *et al.*, Phys. Lett. **107B**, 290 (1981).

[6] G. Gidal, in *VII International Workshop on Photon-Photon Collisions* (World Scientific, 1986).

[7] C. Berger *et al.*, Z. Phys. C **33**, 351 (1987).

[8] S. Brodsky *et al.*, Phys. Rev. D **19**, 1418 (1979).

[9] P. Aurenche *et al.*, Z. Phys. C **29**, 423 (1985).

[10] N. Arteaga-Romero *et al.*, Z. Phys. C **32**, 105 (1986).

[11] C. Zeitlin, *Jet Production in Photon-Photon Collisions at PEP*, PhD thesis, University of California,Davis, 1988. UCD-88-26.

[12] H. Aihara *et al.*, IEEE Trans. Nucl. Sci. **NS30**, 64,67,76,117,153,162 (1983).

[13] M. Cain *et al.*, Phys. Lett. **147B**, 232 (1984).

[14] B. Anderson *et al.*, Phys. Rep. **97C**, 31 (1983).

Sample	Data	QPM	3-jet
Untagged	674 ± 37	$125 \pm 8 \pm 40$	$26 \pm 1 \pm 4$
Tagged	84 ± 9	$44 \pm 4 \pm 10$	$7 \pm 1 \pm 2$

Table 1. Number of events in the region $2 < p_t < 3\,\mathrm{GeV}$ for data and Monte Carlo samples, including systematic errors on the Monte Carlo predictions.

Figure Captions

1. Jet p_t distribution for data for both untagged (a) and tagged (b) samples. The curves represent the expectations for VDM + QPM, as explained in the text. Errors are statistical only.
2. $R'_{\gamma\gamma}$ for the untagged sample (a) and tagged sample (b). In both, $R'_{\gamma\gamma} = 1$ represents the prediction of VDM + QPM. Errors are statistical only.
3. Thrust distributions for the two data samples in the range $2 < p_t < 3\,\mathrm{GeV}$, compared to QPM (2-jet events) normalized to the number of data events. Errors are statistical only.
4. QCD multi-jet diagrams expected to contribute to the high-p_t cross section.
5. Thrust distributions as in Fig. 3, but compared to the sum of absolutely normalized QPM and a 3-jet model normalized to account for the excess. Errors are statistical only.

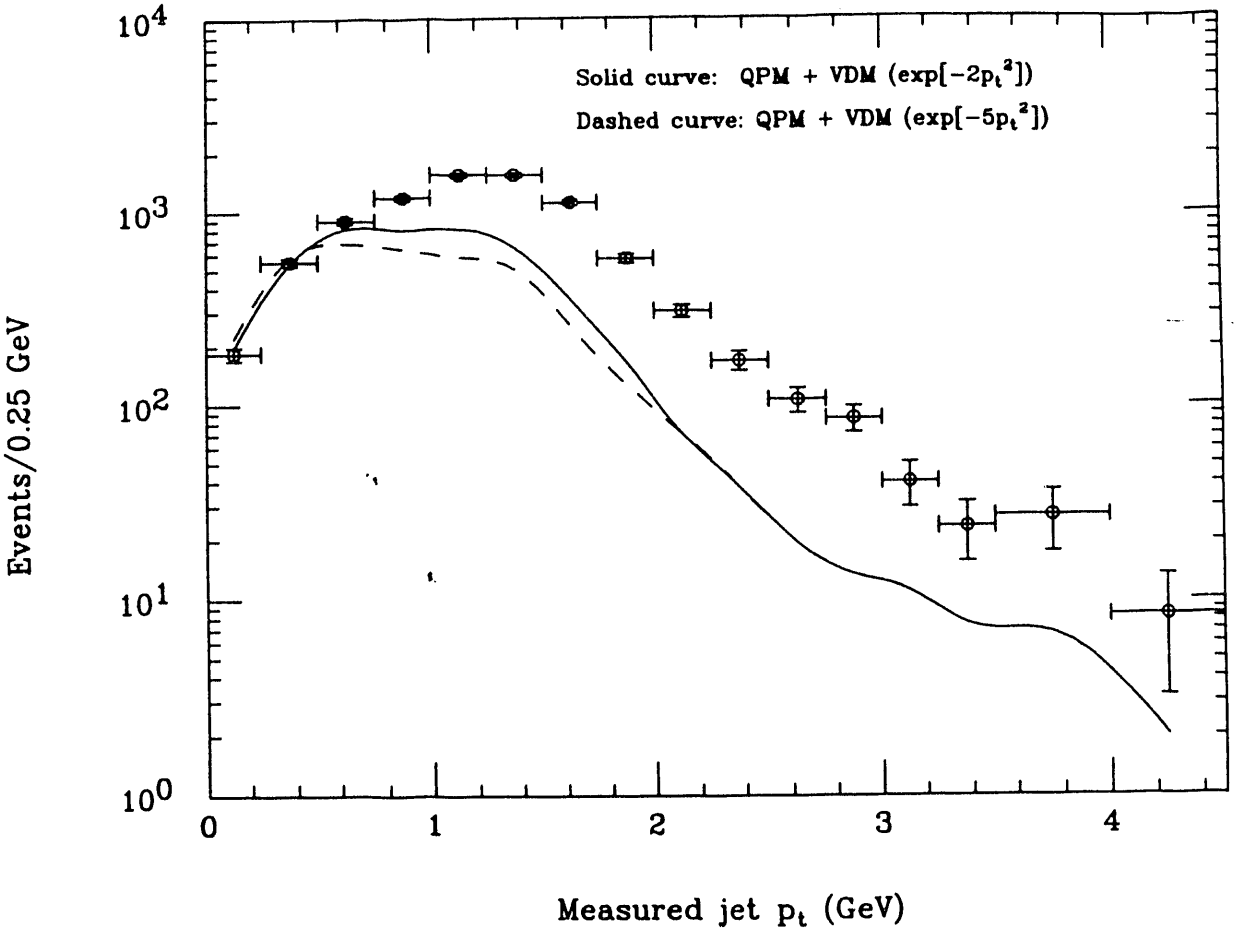
Solid curve: QPM + VDM (exp[−2p_t²])
Dashed curve: QPM + VDM (exp[−5p_t²])
Events/0.25 GeV
Measured jet p_t (GeV)
10^4
10^3
10^2
10^1
10^0
0
1
2
3
4

Figure 1a

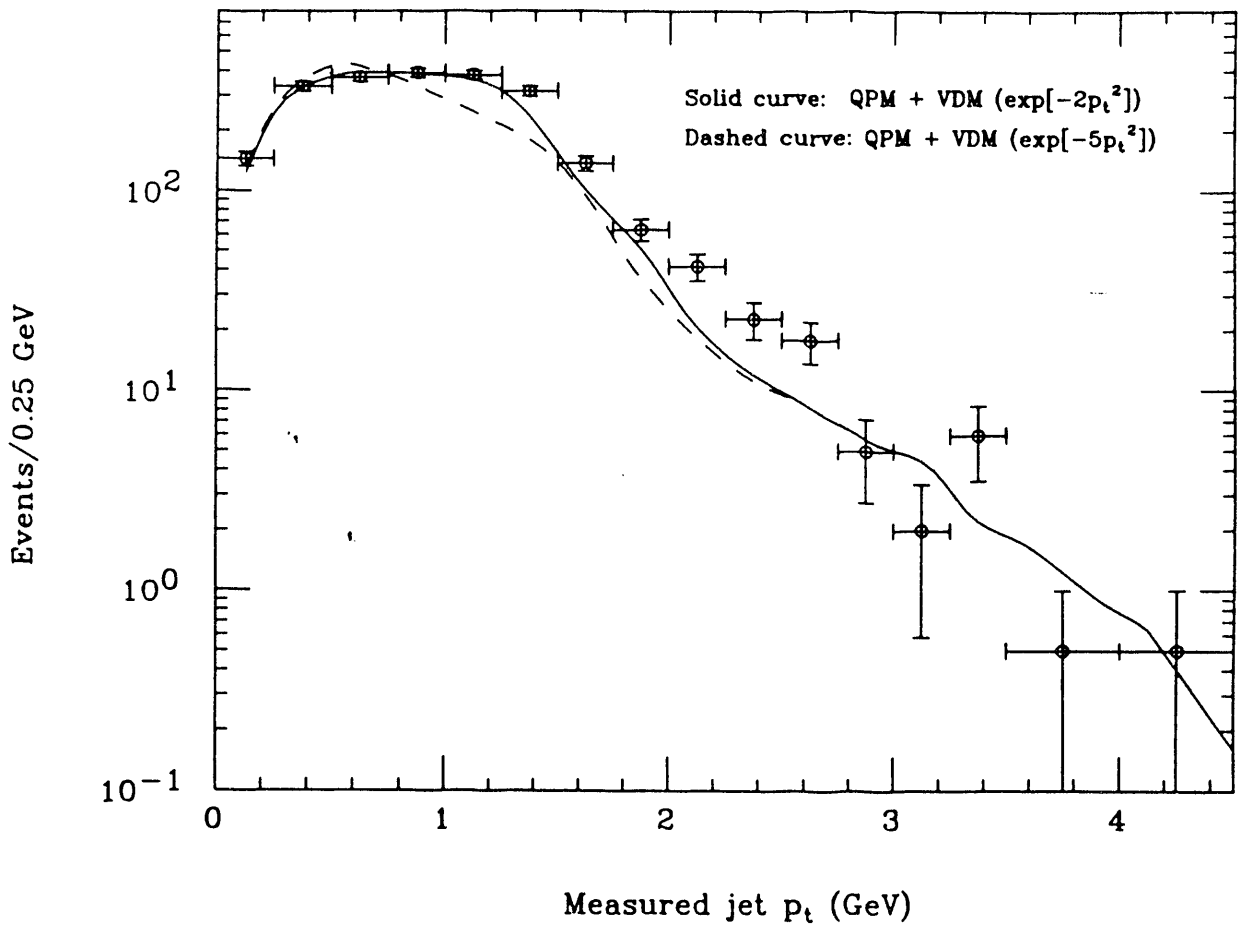
Solid curve: QPM + VDM (exp[−2p_t²])
Dashed curve: QPM + VDM (exp[−5p_t²])
Events/0.25 GeV
10²
10¹
10⁰
10⁻¹
0
1
2
3
4
Measured jet p_t (GeV)

Figure 1b

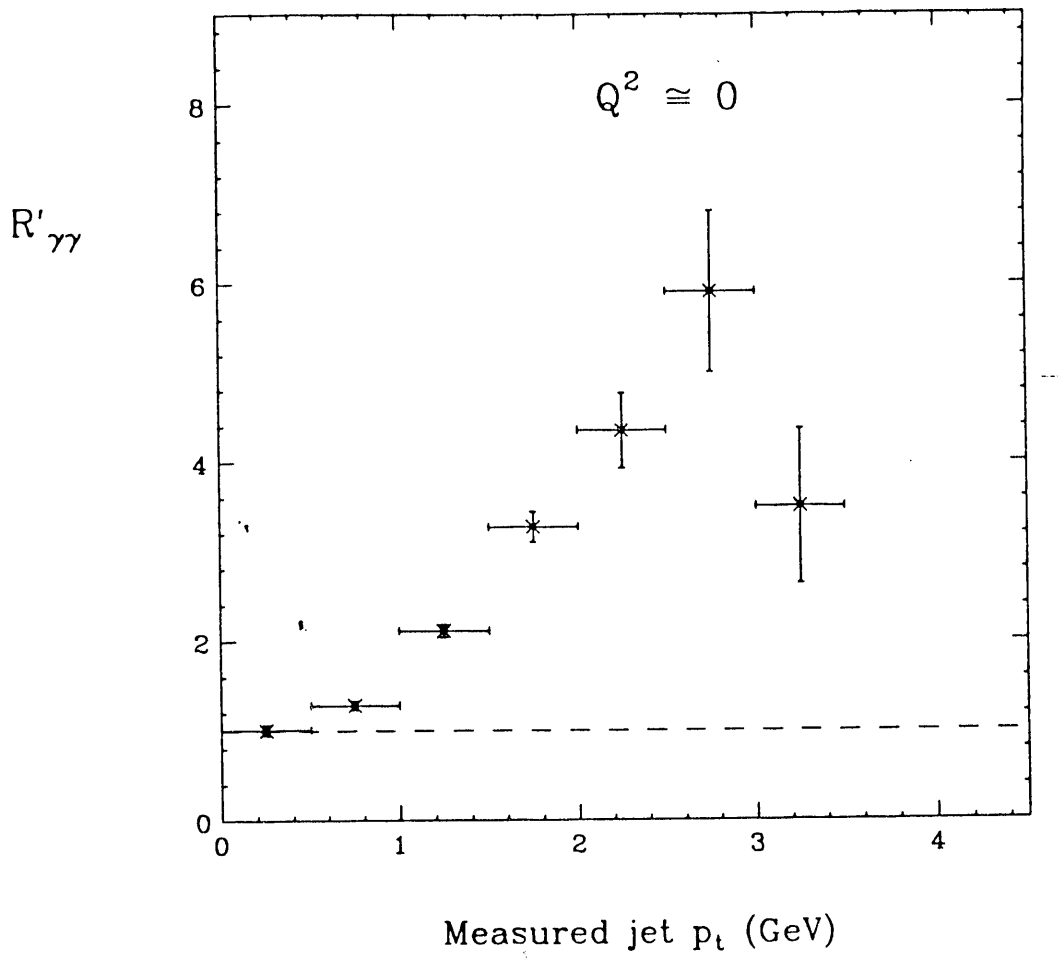

Figure 2a

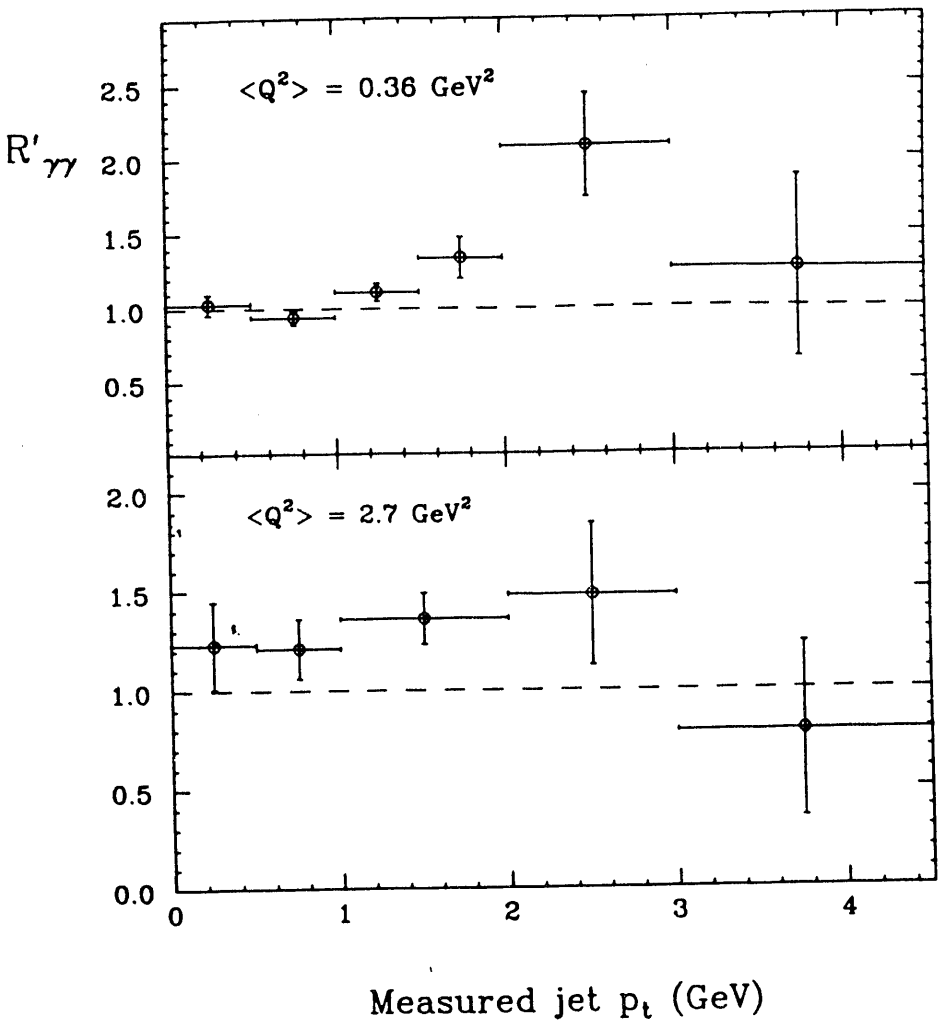
$R'_{\gamma\gamma}$
$\langle Q^2 \rangle$ = 0.36 GeV^2
$\langle Q^2 \rangle$ = 2.7 GeV^2
2.5
2.0
1.5
1.0
0.5
0.0
0
1
2
3
4
Measured jet p_t (GeV)

Figure 2b

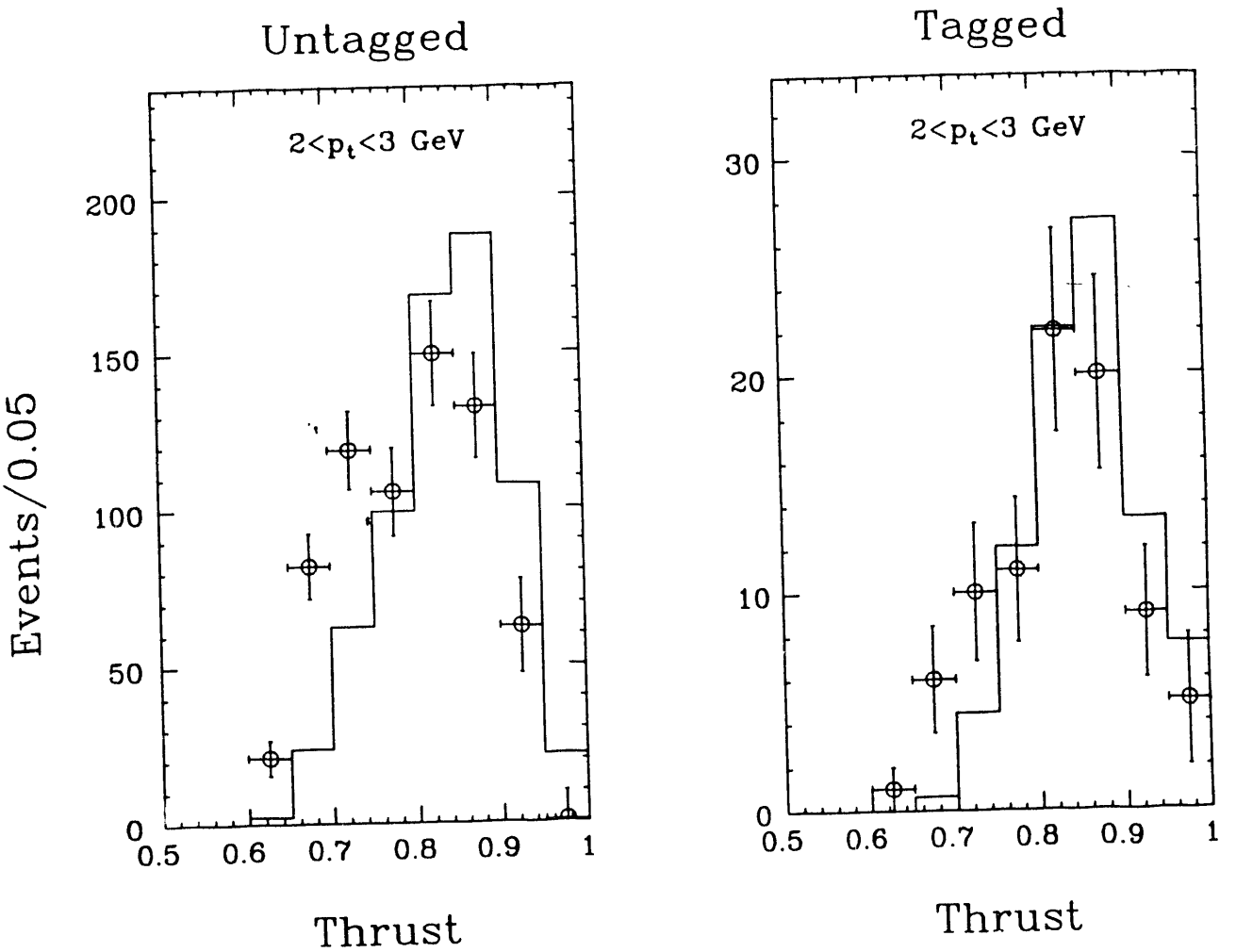
Untagged
2<p_t<3 GeV
Events/0.05
200
150
100
50
0
0.5
0.6
0.7
0.8
0.9
1
Thrust
Tagged
2<p_t<3 GeV
30
20
10
0
0.5
0.6
0.7
0.8
0.9
1
Thrust

Figure 3

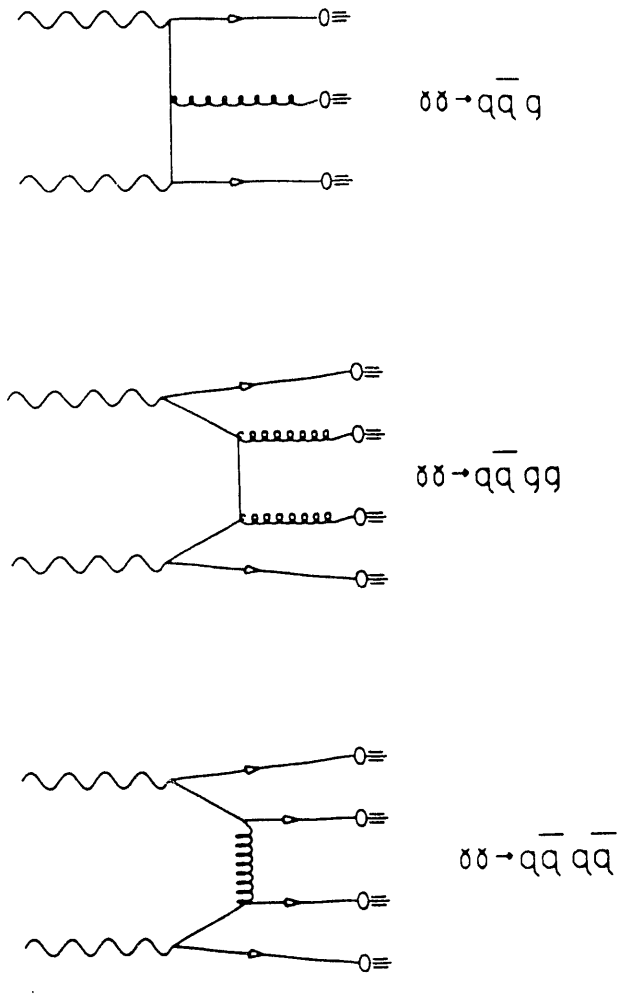

Figure 4

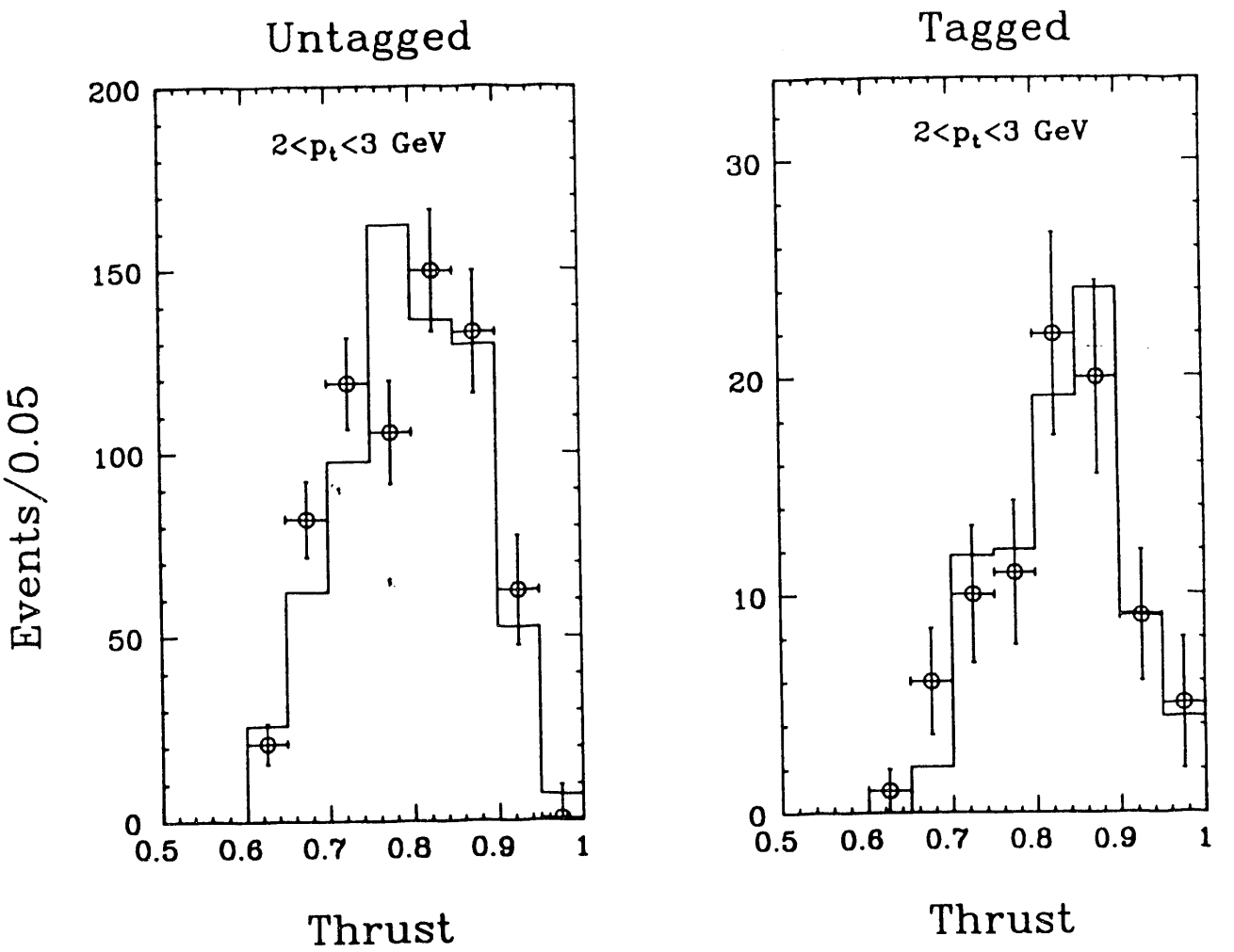
Untagged
Tagged
2<p_t<3 GeV
2<p_t<3 GeV
Events/0.05
Thrust
Thrust
200
150
100
50
0
30
20
10
0
0.5
0.6
0.7
0.8
0.9
1

Figure 5

DATE
FILMED
12/01/93
END